RSC Advances

PAPER

View Article Online
View Journal | View Issue

Cite this: *RSC Adv.*, 2014, **4**, 54953

Probing luminescent Fe-doped ZnO nanowires for high-performance oxygen gas sensing application†

Rishi Vyas,*[ab] Pawan Kumar,[c] Jaya Dwivedi,[c] Sarla Sharma,[d] Shabana Khan,[e] R. Divakar,[f] Avneesh Anshul,[cg] K. Sachdev,[b] S. K. Sharma[a] and Bipin Kumar Gupta*[c]

Received 13th August 2014
Accepted 6th October 2014

DOI: 10.1039/c4ra08586h

www.rsc.org/advances

Herein, we demonstrate the growth of Fe-doped ZnO nanowires using a typical vapour phase transport process for oxygen gas sensing application. The morphologies of these nanowires have been evaluated by high-resolution transmission electron microscopy, which confirms the formation of ZnO nanowires with 20–50 nm diameter and with a *d*-spacing of ~0.270 nm, corresponding to (002) planes. The energy dispersive X-ray spectroscopy result reveals the presence of Fe, Zn and O elements in 9 wt% Fe-doped ZnO nanowires. The Raman and photoluminescence spectroscopy results explore the oxygen deficient structure of these nanowires with Fe ion occupying tetrahedral sites in the ZnO lattice along with some interstitial Zn and Fe ions. Furthermore, these nanowires arrays illustrate a sensitivity of 23 and 31 with fast response/recovery times of about 38 s/46 s and 11 s/11 s at an operating temperatures of 100 °C and 140 °C, respectively. The obtained results established that these luminescent ZnO nanowires could be an excellent choice for high-performance oxygen gas sensing application.

1. Introduction

Nanoscale zinc oxide (ZnO) is futuristic material for their outstanding physical properties and its potential strategic applications. One-dimensional (1D) nanostructures like quantum wires are ideal system to be used as functional components in the fabrications of nanoscale electronic devices. ZnO nanowires exhibit a high surface to volume ratio, which provides a suitable platform for the development of high-performance gas sensing devices.[1,2] The transition metal doping of ZnO is a popular approach for achieving a better performance for device applications, and therefore Fe-doped ZnO nanowires are expected to address several problems *viz.* high response/recovery time, low sensitivity and high operating temperature over their thin film counterpart.[3–6] Electronic charge transfer in n-type ZnO gas sensors can be tuned by altering the doping levels for increased sensitivity towards oxidizing gases such as oxygen.[7,8] Fe-doping induces disorder in the ZnO lattice, which in turn affects the charge transfer to ions absorbed at the surface states of ZnO nanowires.[9] The conductivity of ZnO nanowires is enhanced due to modified density of states facilitated by the addition of Fe.[7] Oxygen gets adsorbed as O^- and O^{2-} ions at metal oxide nanowire surface sites that exhibit both Fe and Zn ion sites, which results in the modification of electronic transfer through the Fe ions.[10] The interaction of gas molecules with Fe ions leads to a change in conductivity that plays an important role in determining the sensitivity, response time and operating temperature of the Fe-doped ZnO nanowire sensor.[11]

Furthermore, it is also interesting to explore the optical properties (photoluminescence) of Fe-doped ZnO nanowires. In general, semiconductors having a large band gap, such as ZnO is widely studied for optical and opto-electronic applications. ZnO nanowires have a lower threshold with radiative recombination occurring near the band edges because of carrier confinement.[12] Emission near band edges are highly dependent on structural defects. The doping of Fe in ZnO nanowires reduces radiative recombination by the incorporation of Fe^{2+}/Fe^{3+} ions, which modifies the carrier concentration.[9,13] Both the photo-generated carrier transit time and response time for effective gas sensing are subsequently reduced. Moreover, pristine ZnO acts as an intrinsic semiconductor with an empty Zn $4s^2$ orbital along with an oxygen $2p^6$ orbital. The transition metal doping and oxygen deficiency increase the effective zinc $4s^2$ electrons that can be easily ionised.[14] Consequently, the performance of ZnO nanowire based sensors can be modified by

[a]*Department of Physics, School of Basic Sciences, Jaipur National University, Jaipur-302017, India. E-mail: mail2rishivyas@gmail.com*

[b]*Department of Physics, Malaviya National Institute of Technology, Jaipur-302017, India*

[c]*CSIR-National Physical Laboratory (CSIR), Dr K S Krishnan Road, New Delhi 110012, India. E-mail: bipinbhu@yahoo.com*

[d]*Department of Physics, Jagan Nath Gupta Institute of Engineering and Technology, Jaipur-302022, India*

[e]*Mechanical Metallurgy Division, Bhabha Atomic Research Centre, Mumbai 400085, India*

[f]*Physical Metallurgy Group (MMG), Indira Gandhi Centre for Atomic Research, Kalpakkam-603102, India*

[g]*CSIR-Advanced Materials and Process Institute, Bopal, 462026, India*

† Electronic supplementary information (ESI) available. See DOI: 10.1039/c4ra08586h

the concentration of defect.[2] Moreover, the band-to-band electronic transitions are enhanced by Fe-doping at lattice sites for reducing charge trapping.[15]

In the present work, a luminescent Fe-doped ZnO nanowire based oxygen gas sensor has been investigated for fast response/recovery time. The ZnO nanowires were synthesized by employing an alternative approach using Fe and Zn as starting materials in a controlled environment for the growth of free standing Fe-doped ZnO nanowires in contrast to the catalyst coated substrates used for obtaining ZnO nanowires during a typical vapour phase transport process.[16,17] The morphology of the synthesized ZnO nanowires was examined by using transmission electron microscopy (TEM). The micro-chemical analysis was carried out by energy dispersive X-ray spectroscopy (EDS) for the estimation of the elemental proportion of Fe, Zn and O in the sample. The structural and optical properties of ZnO nanowires have been investigated using X-ray diffraction (XRD), selective area electron diffraction pattern (SAED), Raman scattering and photoluminescence (PL), as well as time-resolved spectroscopy. The photoluminescence investigations results also support the cause for the enhancement of the high-performance gas sensing for Fe-doped ZnO nanowires. This is because Fe-doping enhances the oxygen vacancies, which are clearly observed from the strong green PL emission intensity. These vacancies are highly desired to create more active sites to absorb oxygen gas. The current–voltage (I–V) and oxygen sensing measurements demonstrate the high sensitivity and fast response/recovery time at lower operating temperatures.

2. Experimental

2.1 Synthesis of Fe-doped ZnO nanowires and plausible growth mechanism

In the present investigation, the precursor materials Zn and Fe fine powder (99.99% purity, 50 nm grain size) were purchased from Sigma-Aldrich Corp. to grow Fe-doped ZnO nanowires. One gram of metallic Zn powder was mixed with different concentrations (1, 4, 7, 9 and 10 wt%) of Fe powder and the mixture was placed in an alumina boat to load at the centre of the 2 inch diameter quartz tube in a split furnace for the growth of the Fe-doped ZnO nanowires. Prior to the synthesis experiment, initially the quartz tube was maintained under rotary vacuum $\sim 10^{-2}$ Torr to remove moisture, and then purged with continuous nitrogen flow up to 900 °C at 1 atm pressure. Then, the furnace was programmed to raise the temperature from 25 to 900 °C in 3 h, to maintain 900 °C for 30 min, and then cooled from 900 to 25 °C in 5 h. The quartz tube was purged with argon flow (500 sccm) until it reached 100 °C, while a constant flow of 500 sccm containing 5% oxygen in argon was maintained from 400 °C onwards until it cooled to 400 °C. The outlet of furnace was passed through a 500 ml water bottle filled with deionised water to maintain the excess ZnO vapor density high at the cool end of the tube. At 900 °C formation of a web-like structure was observed at the end of the tube (which is at room temperature) that becomes denser as the reaction progressed. A part of the web was collected on a quartz substrate with the help of tweezers and drops of silver paste were used to firmly place this nanowire bundle from its ends. This silver paste was further used to form contacts for obtaining gas sensing and current–voltage (I–V) characteristics. A part of this nanowire bundle was separately collected for other measurements. The schematic diagram of the actual set-up is shown in Scheme 1a. The optical image and surface morphology of the actual gas sensing device is shown in Scheme 1b and c, respectively; the marked red arrow in Scheme 1b exhibits the place where the SEM image has been taken. For more clarity, the magnified view of the Scheme 1c is also shown in Fig. S1 (see ESI†). The systematic experimental results reveal that 9 wt% Fe was the optimum concentration for the efficient growth of Fe-doped ZnO nanowires. Beyond 9 wt% of Fe suppresses the ZnO nanowire growth and below 9 wt% results in the under growth of Fe-doped ZnO nanowires, which can be easily observed form the surface morphology and microstructural information of different concentrations (1 wt% and 10 wt% Fe in ZnO nanowires) of Fe-doped ZnO nanowires as shown in Fig. S2(a)–(d) (see ESI†). In Fig. S2(a) and (b),† the red cross marked circle represents the under growth morphology of 1 wt% Fe doped ZnO nanowires and cluster formation of 10 wt% Fe doped ZnO nanowires.

The well-established growth mechanism of ZnO nanostructures reported in the literature is the self-catalyzed vapor–liquid–solid (VLS) technique, which has two important steps: nucleation as the initial stage followed by epitaxial growth. This method results concurrently in heterogeneous and multiple types of nanostructures.[18–21] However, in most of the cases, the self-catalyzed process suffers because of high temperature and mixture product of nanostructures, which limits its extensive use for synthesize by this technique. To overcome this issue, the metal catalyst assisted VLS mechanism could be the best alternative for a 1D growth of single type nanostructures. In the present investigations, the plausible mechanism of Fe-doped ZnO nanowires can be understood by a proposed growth

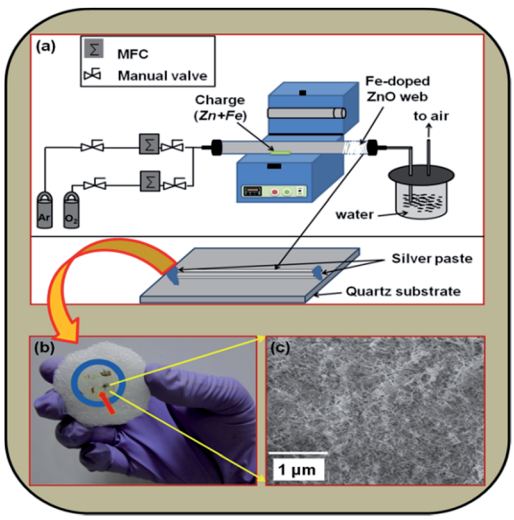

Scheme 1 (a) The schematic diagram of actual set-up, (b) optical image (c) surface morphology of Fe doped ZnO nanowire gas sensing device; the marked red arrow in (b) exhibits the place where the SEM image has been taken.

mechanism in which Fe metal catalyst forms liquid alloy droplets at a high temperature by adsorbing vapor components. During the growth process, the fluctuation of temperature or vapor pressure originates at an intermediate stage and the Fe–Zn–O alloy becomes a solution in which the actual concentration of the components is higher than the equilibrium concentration. Then, it drives the precipitation of the component at the liquid–solid interface to achieve a minimum free energy of the alloy system Fe–Zn–O. As a result, the 1D crystal growth begins, and it continues as long as the vapor components are offered. Vapor (which carries solid components), liquid (catalyst alloy), and solid (precipitated one-dimensional structures) phases are involved. Metal catalysts are essential in the VLS mechanism, but not all metals can work. The metal should meet the following requirements:[22]

(a) It must form a liquid solution with a component of the solid phase; the solubility limit of the catalyst component in the liquid phase must be considerably higher than that in the solid phase. Under this condition, the catalyst easily leads to the formulation of the liquid alloy with little contamination in the solid phase.

(b) The vapor pressure (V_p) of the catalyst component over the liquid alloy should be small. Otherwise, the catalyst will evaporate and eventually disappear in the course of growth.

(c) It must be inert to chemical reactions. Otherwise, a reaction could deprive it of its catalytic function.

(d) It must not make an intermediate solid.

Additionally, the doping of Fe catalyst ZnO improves the active sites for gas sensing applications, which is further evidenced and discussed in the PL spectroscopy and gas sensing sections.

2.2 Characterizations of Fe-doped ZnO nanowires

For phase identification, the structural characterization was performed using XRD (Rigaku: MiniFlex, Cu Kα_1; $\lambda = 1.5406$ Å). The Raman spectrum was obtained with the incident light being normal to the sample surface and all the results have been obtained by the subtraction of signal from the Si substrate used for placing ZnO nanowire bundles using the 363.8 nm UV line of the argon laser. High resolution TEM/TEM (Philips CM-200 TEM) confirms the formation of nanowires. The room temperature photoluminescence studies were carried out using a Perkin Elmer spectrometer (model LS-55) equipped with a xenon lamp and a monochromator source of 325 nm excitation wavelength. Current–voltage (I–V) and oxygen sensing measurements were carried out using a custom built combustible gas sensing facility (CGSF) at materials research laboratory (schematic shown in Fig. 1). This unit consists of a SS chamber housing with a PID controlled heater, which also acts as a substrate holder. The cold water is circulated in the walls of the chamber to prevent it from excess heating. The Cu pressure contacts were used to make contact with the sensing layer. A constant gas flow (100 sccm) is maintained using mass flow controllers (Aalborg-DFC) and the chamber is evacuated with a rotary vacuum pump to maintain a constant pressure of 0.28 mbar throughout the gas sensing, as well as I–V measurements. The system is configured for a two-point measurement system and is driven with a voltage source. Current measurement is performed by a Keithley 2400 SMU system, which is interfaced to a computer using National Instrument's LabVIEW software.

3. Results and discussions

The gross structural analyses of undoped and Fe-doped ZnO are characterized using XRD. Fig. 2(a) shows the XRD patterns of the 9 wt% Fe-doped ZnO nanowires. It can be seen that the samples exhibit a hexagonal wurtzite phase with the space group $P6_3mc$ (JCPDS no. 36-1451) and no secondary phase was found. The XRD patterns of the undoped and Fe-doped ZnO are also shown in Fig. S3 (see ESI†). The major intense peaks of the XRD pattern show a slight shifting of the center of the diffraction peaks toward a lower angle in comparison to that of the undoped ZnO sample (Fig. S3†). The shifting of the XRD peaks with the doped ZnO indicates that Fe^{2+} has been effectively substituted into the ZnO host structure at the Zn^{2+} site. The lattice parameter of 9 wt% Fe-doped ZnO nanowire is slightly deviated from the standard JCPDS card; $a = b = 3.2468$ Å, $c = 5.2036$ Å. The estimated lattice parameters of 9 wt% Fe-doped ZnO nanowire are $a = (3.2518 \pm 0.0037)$ Å, $c = (5.2098 \pm 0.0021)$ Å, which are slightly larger than those of undoped ZnO $a = (3.2509 \pm 0.0045)$ Å, $c = (5.2060 \pm 0.0019)$ Å. The obtained XRD results are consisted with earlier reported results for liquid polyols Fe-doped ZnO nanoparticles.[23]

The Raman spectrum of Fe doped ZnO nanowires was obtained by exciting the sample using a 363.8 nm argon ion laser as shown in Fig. 2(b). Two prominent peaks at 330 and 436 cm^{-1} originate from the $2E_2$ mode and nonpolar optical phonon mode (E_2), respectively.[24,25] The high intensity nonpolar

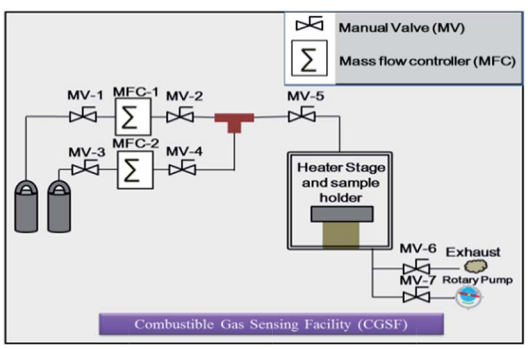

Fig. 1 Combustible gas sensing facility (CGSF).

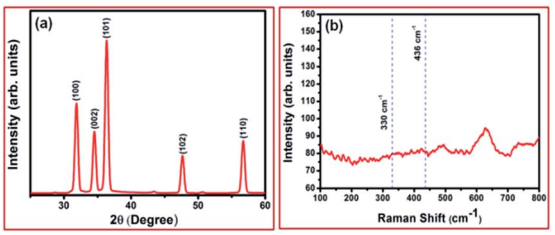

Fig. 2 XRD and Raman spectrum of 9 wt% Fe-doped ZnO nanowires.

optical phonon mode (E_2) of ZnO nanowires is generally attributed to the oxygen deficiency. However, in this case, it indicates the presence of interstitial transition metal ions (Zn^{2+}, Fe^{2+}/Fe^{3+}) because of the high doping concentration.[26] Other transverse and longitudinal optical polar modes appear as small peaks in the spectra indicative of weak electron phonon coupling. The full width at half maximum (FWHM) of the E_2 high mode is 10.12 cm^{-1} indicating the presence of Fe ions at the tetrahedral lattice site of the wurtzite ZnO structure.[26,27] The presence of oxygen deficient nanowires because of Fe ion incorporation is also confirmed by the existence of corresponding vibration modes as indicated in the Fig. 2(b), which is consistent with earlier reported results.[26] The other less intense vibration mode in the Raman spectra is because of the occupancy of Fe^{3+} ions at Zn^{2+} site, resulting in host lattice defect and internal strains due to different growth directions.[28]

The microstructure analysis was carried out with a TEM/HRTEM instrument. The bright field image of nanowires is shown in Fig. 3(a), which suggests the formation of nanowires having diameter in the range from 20–50 nm. The selected area electron diffraction (SAED) pattern of nanowires is shown in Fig. 3(b), which matches well with the zinc oxide hexagonal wurtzite phase with the space group $P6_3mc$ (JCPDS no. 36-1451). The SAED pattern exhibits the discontinuous and distinct bright rings, which confirms the oriented crystalline nanostructure. The TEM image displayed in Fig. 3(c) clearly illustrates the secondary growth on primary ZnO nanowires in different orientations. The incorporation of Fe in ZnO as Fe^{2+}/Fe^{3+} must have resulted in the various growth sites enabling the growth of different crystallographic planes at the top of one another. The Fig. 3(d) exhibits the typical HRTEM image and corresponding lattice fringes of 9 wt% Fe-doped ZnO nanowires. The *d*-spacing, calculated from the HRTEM image, as well as from electron diffraction pattern for (002) plane are 0.269 and 0.271 nm, respectively. We also evaluated the morphology and microstructural changes with respect to different concentrations of Fe doping as shown in Fig. S2(a)–(d).† It is interesting to note that SEM and TEM image of 1 wt% Fe-doping clearly exhibits the under growth situation of Fe-doped ZnO nanowires, as shown in Fig. S2(a) and (c).† The SEM and TEM images of 10 wt% Fe-doping represent the cluster formation of Fe doped ZnO nanowires, as shown in Fig. S2(b) and (d).† Thus, the result of high concentration Fe-doping above 9 wt% clearly demonstrates the clusters of unconsumed Fe nanoparticles, which suppress the growth of Fe-doped ZnO nanowires. As a result, the PL intensity and gas sensing both are reduced, which is further systematically evidenced in the PL and gas sensing section for different concentrations (1, 4, 7, 9 and 10 wt%) of Fe-doping in ZnO nanowires.

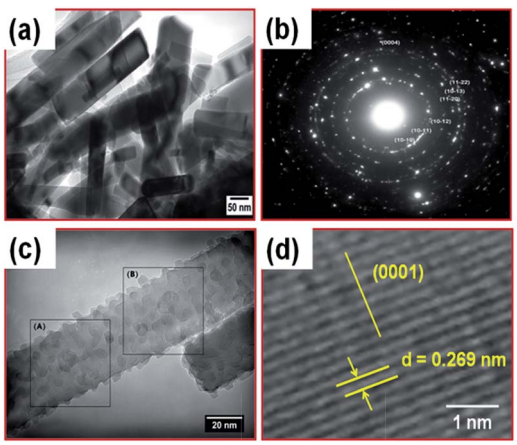

Fig. 3 (a) Bright Field image showing 9 wt% Fe-doped zinc oxide nanowires with diameter in 20–50 nm range and length in 200–500 nm range, (b) SAED pattern corresponding to a bunch of nanowires, (c) TEM image of 9 wt% Fe-doped ZnO nanowires, the rectangular marked region A & B clearly represents the secondary growths on primary ZnO nanowire in different orientations and (d) typical HRTEM image of 9 wt% Fe-doped ZnO nanowires.

The atomic concentration of host ZnO and dopant Fe are quantitatively analysed from the energy dispersive X-ray spectroscopy (EDS). Fig. 4 demonstrates the EDS spectrum of 9 wt% Fe-doped ZnO nanowires. The EDS spectrum signifies the presence of Zn, O and Fe elements. Additionally, we also performed the compositional studies on the stoichiometry of 9 wt% Fe-doped ZnO nanowires. The EDAX spectrum indicates the presence of Zn, O and Fe elements. Additionally, we also performed the compositional studies on the stoichiometry of 9 wt% Fe-doped ZnO nanowires. The Table 1 shows the atomic/weight percent of different elements present in Fe-doped ZnO nanowires. The micro-chemical analysis confirmed 7.43% atomic (8.22 wt%) of Fe in ZnO. The obtained result is in good agreement with the amount of Fe utilized to dope (9 wt%) in this experiment. Microscopic studies illustrated the presence of Fe at the lattice sites nullifying the possibility or signature of its presence at the surface or on grain boundaries.

In order to explore the detailed optical property of these nanowires, we have carried out photoluminescence (PL) and time-resolved spectroscopy. For the optimization, the PL emission spectra corresponding to the different concentration of Fe in ZnO nanowires is shown in Fig. S4.† The PL results reveal that the peak position and the shape of the emission spectrum are identical for all the samples, but intensity is maximum for 9 wt% Fe-doped ZnO nanowires. The emphasis has been put on the near band edge region for understanding the optical property of the system. Fig. 5(a) exhibits the excitation spectra of 9 wt% Fe-doped ZnO nanowires. The broad peak at 325 nm

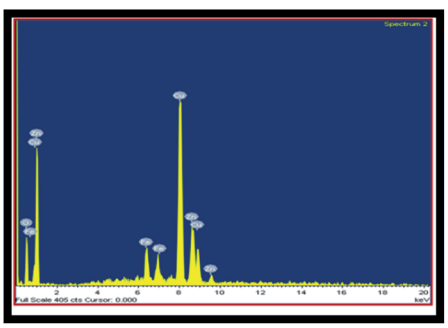

Fig. 4 Energy dispersive X-ray spectrum of Fe-doped ZnO nanowires.

Table 1 EDS table of 9 wt % Fe doped ZnO nanowires.

Elements	OK	FeK	CuK	ZnK	Total
Weight%	8.48	8.22	64.80	18.50	100
Atomic%	26.78	7.43	51.50	14.29	100

corresponds to the defects site in Fe-doped ZnO nanowire and the peak at 378 nm corresponds to the band edge of Fe-doped ZnO at 498 nm fixed emission. Fig. 5(b) demonstrates the emission spectrum of 9 wt% Fe-doped ZnO corresponding to excitation at 325 nm. The broad emission spectrum centred at 498 nm can be attributed to donor-bound-excitations of a n-type semiconductor.[29] The CIE (chromaticity diagram) color coordinates obtained from the emission spectrum of 9 wt% Fe-doped ZnO, upon 325 nm excitation wavelength, are $x = 0.2321$ and $y = 0.4300$, as shown in Fig. 5(c). Fig. 5(d) exhibits the emission spectra of undoped ZnO and 9 wt% Fe-doped ZnO nanowires corresponding to the excitation at the band-edge ultraviolet peak at 378 nm, which results in a prominent strong green emission peaking at 498 nm wavelength. The influence of oxygen partial pressure on the optical transitions of oxides is quite apparent in the form of the above-mentioned strong green emission. The surface states of nanostructured materials are known to critically affect the luminescence properties of the materials. The emission peak at 498 nm can be correlated to the excitons bound to the structural defects.[30] The Fe doping generates defects at band-edges because of the interionic transition of photo carriers between Fe^{3+} and O^{-}/O^{2-} ions.[31] The concentrated defect resulting in the strong green emission because of the radiative recombination of a photo-generated hole with an electron attributed to an oxygen vacancy in ZnO. The increase in the emission intensity is because of the Fe-doping at the lattice site as shown in Fig. 5(d). The CIE (chromaticity diagram) color coordinates obtained from the emission spectrum of 9 wt% Fe-doped ZnO upon 378 nm excitation wavelength are $x = 0.2131$ and $y = 0.4177$, as shown in Fig. 5(e). The decay was recorded for the transition at 498 nm emission corresponding to 378 nm excitation by a time-correlated single photon counting technique by using a xenon flash lamp as a source of excitation. The life-time data obtained from 9 wt% Fe-doped ZnO nanowires was best fitted to a double-exponential function as,

$$I_0 = A_1 \exp(-t/\tau_1) + A_2 \exp(-t/\tau_2) \quad (1)$$

where τ_1 and τ_2 are the decay life-times of the luminescence, and A_1 and A_2 are the weighting parameters. The lifetime data of 9 wt% Fe-doped ZnO nanowires is shown in Fig. 5(f). The inset of Fig. 5(f) demonstrates the exponential fitting of decay profile as described in eqn (1). The parameters generated from fitting are listed in the inset of Fig. 5(f). The observed life-times are $\tau_1 \sim 1.65$ μs and $\tau_2 \sim 14.25$ μs. For double-exponential decay, the average life-time (τ_{av}) is usually tailored to substitute the various components of the luminescence life-time, which is determined by the following equation.[32,33]

$$\tau_{av} = (A_1\tau_1^2 + A_2\tau_2^2)/(A_1\tau_1 + A_2\tau_2) \quad (2)$$

The average life-time for 9 wt% Fe-doped ZnO nanowires synthesized here is calculated as $\tau_{av} \sim 13$ μs. The obtained result is highly-suitable for several optoelectronic device applications.

Finally, the gas sensing performance of a fabricated device was evaluated and a plausible mechanism has been discussed in detail. The oxygen gas sensing performance of Fe-doped ZnO nanowires as a unidirectional array was examined in a control atmosphere at different operating temperatures using DC resistance measurements. The ZnO nanowires showed measurable change in resistance when exposed to oxygen gas indicating a typical n-type semiconductor behaviour. The oxygen gas sensing performance of undoped and 9 wt% Fe-doped ZnO nanowires is shown in Fig. 6. Fig. 6(a) exhibits oxygen gas sensing characteristics, which correspond to an operating temperature of 100 °C, whereas Fig. 6(b) corresponds to 140 °C for the undoped ZnO sample. The Fig. 6(c) exhibits oxygen gas sensing characteristics, which corresponds to an operating temperature of 100 °C, whereas Fig. 6(d) corresponds to 140 °C for 9 wt% Fe-doped ZnO nanowires. The obtained results clearly demonstrates the enhancement in the gas sensing properties of ZnO after doping. For better

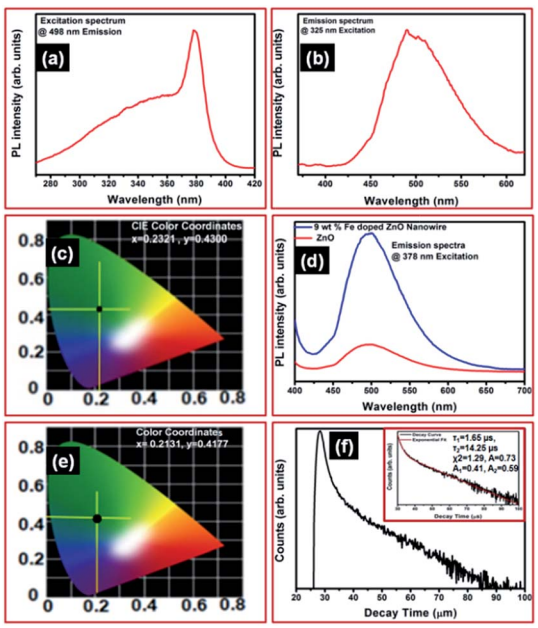

Fig. 5 (a) PL excitation spectrum of 9 wt% Fe-doped ZnO nanowires at 498 emission wavelength, (b) PL emission spectrum of 9 wt% Fe-doped ZnO nanowires at 325 excitation wavelength and (c) color coordinates of 9 wt% Fe-doped ZnO nanowire (excitation at 325 nm), (d) PL emission spectra of undoped ZnO and 9 wt% Fe-doped ZnO nanowires at 378 excitation wavelength, (e) color coordinates of 9 wt% Fe-doped nanowires (excitation at 378 nm) and (f) TRPL decay profile of 9 wt% Fe-doped nanowires recorded at room temperature while monitoring the emission at 498 nm at excitation wavelength of 378 nm; inset shows the lifetime data and the parameter generated by the exponential fitting curve.

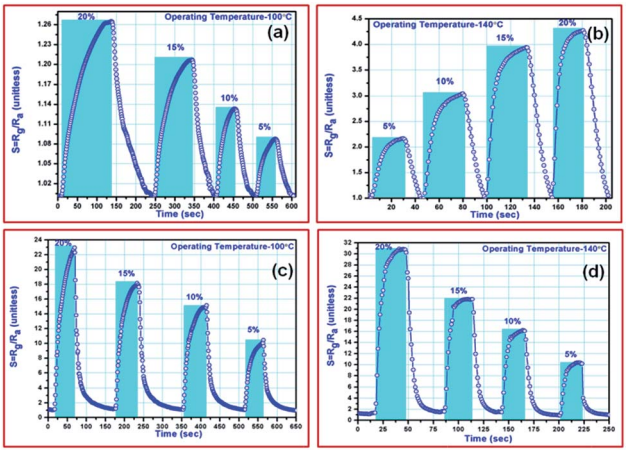

Fig. 6 (a and b) Oxygen sensing characteristics for undoped ZnO at operating temperatures of 100 °C and 140 °C, respectively. (c and d) Oxygen sensing characteristics for 9 wt% Fe-doped ZnO nanowire at operating temperatures of 100 °C and 140 °C, respectively.

understanding the obtained results of doped and undoped sample is also compared in Table TS1 in the ESI.† We have also evaluated the gas sensing properties at different concentrations (1, 4, 7, 9 and 10 wt%) of Fe in ZnO nanowires as shown in Fig. S5.† The obtained result reveals that the gas sensing performance gradually improves with increase in concentration up to 9 wt% Fe doping. It has been observed that the gas sensing performance decreases further at higher concentration. The decrease in PL and gas sensing performance after 9 wt% originates because of unconsumed Fe particles during the growth of Fe-doped ZnO nanowires. The presence of unused Fe clusters quenches the luminescence and also produces a blocking effect on gas sensing performance. The obtained result is consistent with our microstructural results.

The oxygen sensitivity of ZnO nanowires was measured in terms of resistance offered by nanowires in the presence of a known concentration of oxygen in nitrogen and in pure nitrogen. Response and recovery times from 9 wt% Fe-doped ZnO nanowire were measured as (38 ± 1) s and (46 ± 1) s at 100 °C, and (11 ± 1) s and (11 ± 1) s at 140 °C, respectively. The current–voltage (*I–V*) characteristics exhibited an ohmic nature within the full range of applied voltage and current ranges measured at 100 °C and 140 °C. Response and recovery times from undoped ZnO was measured as (81 ± 1) s and (74 ± 1) s at 100 °C, and (12 ± 1) s and (19 ± 1) s at 140 °C, respectively.

The outcome of a typical potential sensor device primarily depends on the interaction of the test gas and sensing layer. The high surface to volume ratio and 9 wt% Fe-doping is capable of enhancing gas sensing capacity and response/recovery time of sensors by increasing the effective number of active sites for gas interaction at the given operating temperature. On oxygen exposure to the sensing layer, the oxygen atoms diffuse into the sample and get adsorbed at the active sites. The adsorbed oxygen atoms at the surface compensates surface vacancies, which instantaneously increases the resistance of the nanowires.[10] The oxygen deficiency and defects on the surface act as oxygen absorption sites.[34] The lattice distortion because of the presence of mixed state of Fe^{2+} and Fe^{3+} ions modifies the band structure and Fermi level.[7] The increase in electron density and active surface states with increased temperature leads to fast response at higher temperature, which explains the fast response/recovery time and high sensitivity at an operating temperature of 140 °C compared to 100 °C. Further, 9 wt% Fe in the lattice provides the carrier electrons a quantum mechanical path for current flow by electron hopping between Fe^{3+} and Fe^{2+} similar to the ferrites, which also contribute to the fast response/recovery of the 9 wt% Fe-doped nanowire sensor. The problem of charge trapping at the oxygen band gap in the conventional oxygen gas sensor devices can also be addressed by Fe doping. In the spinal lattice, the Fe^{3+} electrostatic interaction, Zn deficiency and other disorder giving rise to Fe^{2+} ions leads to deviations from ferrite stoichiometry.[35]

Thus, the facile strategy to synthesized Fe-doped nanowires provides an economically viable route for large scale synthesis. Furthermore, the obtained high-performance gas sensing characteristics of 9 wt% Fe-doped ZnO nanowires promise their potential use in making portable gas sensing devices, which are highly comparable with the reported gas sensors for other materials.[36]

4. Conclusions

We have systematically investigated the structural and optical properties of the as-synthesised 9 wt% Fe-doped ZnO nanowires. The Fe-doped ZnO nanowires were concluded to possess Fe^{2+}/Fe^{3+} ions at tetrahedral and interstitial sites of the ZnO lattice giving origin to oxygen deficiency in these nanowires. The interaction of oxygen ions with modified active sites because of the presence of Fe^{2+}/Fe^{3+} ion sites modified the charge transport between the ion-adsorbed oxygen and bulk of the ZnO nanowires resulting in fast response/recovery time with high sensitivity at lower operating temperatures. Hence, the obtained gas sensing results of luminescent Fe-doped ZnO nanowires rationalize its potential application in high-performance gas sensing applications.

Acknowledgements

The authors wish to thank Prof. R. C. Budhani, Director, N.P.L., New Delhi for his keen interest in the work. The authors are thankful to Prof. O.N. Srivastava (Banaras Hindu University, Varanasi) for his encouragement. Authors are thankful to University Grants Commission (UGC) for financial help.

References

1 L. Liao, H. B. Lu, J. C. Li, C. Liu, D. J. Fu and Y. L. Liu, *Appl. Phys. Lett.*, 2007, **91**, 173110.
2 M. W. Ahn, K. S. Park, J. H. Heo, J. G. Park, D. W. Kim, K. J. Choi, J. H. Lee and S. H. Hong, *Appl. Phys. Lett.*, 2008, **93**, 263103.

3 S. J. Pearton, D. P. Norton, M. P. Ivill, A. F. Hebard, J. M. Zavada, W. M. Chen and I. A. Buyanova, *IEEE Trans. Electron Devices*, 2007, **54**, 1040–1048.
4 S. Park, S. An, H. Ko, C. Jin and C. Lee, *ACS Appl. Mater. Interfaces*, 2012, **4**, 3650–3656.
5 J. Y. Park, Y. K. Park and S. S. Kim, *Mater. Lett.*, 2011, **65**, 2755–2757.
6 J. Y. Park, S. W. Choi and S. S. Kim, *J. Am. Ceram. Soc.*, 2011, **94**, 3922–3926.
7 S. Gautam, S. Kumar, P. Thakur, K. H. Chae, R. Kumar, B. H. Koo and C. G. Lee, *J. Phys. D: Appl. Phys.*, 2009, **42**, 175406–175412.
8 S. Hasegawa, Y. Susaki and S. Matasuri, *Sens. Actuators, B*, 1993, **14**, 509–510.
9 G. Chen, J. J. Peng, C. Song, F. Zeng and F. Pan, *J. Appl. Phys.*, 2013, **113**, 104503.
10 F. H. Ramirez, J. D. Prades, A. Tarancon, S. Barth, O. Casals, R. J. Diaz, E. Pellicer, J. Rodriguez, J. R. Morante, M. A. Juli, S. Mathur and A. R. Rodriguez, *Adv. Funct. Mater.*, 2008, **18**, 2990–2994.
11 R. K. Sharma, M. C. Bhatnagar and G. L. Sharma, *Sens. Actuators, B*, 1998, **46**, 194–201.
12 D. Banerjee, J. Y. Lao, D. Z. Wang, J. Y. Huang, D. Steeves, B. Kimball and Z. F. Ren, *Nanotechnology*, 2004, **15**, 404–409.
13 K. W. Liu, R. Chen, G. Z. Xing, T. Wu and H. D. Sun, *Appl. Phys. Lett.*, 2010, **96**, 023111.
14 S. Sen, D. Chowdhary and N. A. Kouklin, *Appl. Phys. Lett.*, 2007, **91**, 093125.
15 N. Kouklin, M. Omari and A. Gupta, *Transition metal-doped ZnO nanowires: en route towards multi-colour light sensing and emission applications, nanowires science and technology*, ed. N. Lupu, INTECH, Croatia, 2010, ch. 17.
16 Z. Zhu, T. L. Chen, Y. Gu, J. Warren and R. M. Osgood, *Chem. Mater.*, 2005, **17**, 4227–4234.
17 H. Qi, E. R. Glaser, J. D. Caldwell and S. M. Prokes, *J. Nanomater.*, 2012, **2012**, 260687.
18 Z. L. Wang, *J. Phys.: Condens. Matter*, 2004, **16**, R829–R858.
19 P. Yang, H. Yan, S. Mao, R. Russo, J. Johnson, R. Saykally, N. Morris, J. Pham, R. He and H. J. Choi, *Adv. Funct. Mater.*, 2002, **12**, 323–331.
20 B. K. Gupta, D. Haranath, S. Chawla, H. Chander, V. N. Singh and V. Shanker, *Nanotechnology*, 2010, **21**, 225709.
21 Y. H. Yang, B. Wang and G. W. Yang, *Nanotechnology*, 2006, **17**, 5556–5560.
22 H. J. Choi, *Semiconductor nanostructures for optoelectronic devices, nanoscience and technology*, ed. G. C. Yi, Springer, Verlag, Berlin, Heidelberg, 2012, ch. 1.
23 J. Wang, J. Wan and K. Chen, *Mater. Lett.*, 2010, **64**, 2373–2375.
24 C. Bundesmann, N. Ashkenov, M. Schubert, D. Spemann, T. Butz, E. M. Kaidashev, M. Lorenz and M. Grundmann, *Appl. Phys. Lett.*, 2003, **83**, 1974.
25 H. C. Hsu, C. S. Cheng, C. C. Chang, S. Yang, C. S. Chang and W. F. Hsieh, *Nanotechnology*, 2005, **16**, 297–301.
26 P. Jiang, J. J. Zhou, H. F. Fang, C. Y. Wang, Z. L. Wang and S. S. Xie, *Adv. Funct. Mater.*, 2007, **17**, 1303–1310.
27 J. B. Wang, G. J. Huang, X. L. Zhong, L. Z. Sun, Y. C. Zhou and E. H. Liu, *Appl. Phys. Lett.*, 2006, **88**, 252502.
28 Z. Bin, Z. S. Min, W. H. Wei and D. U. Z. Liang, *Chin. Sci. Bull.*, 2008, **53**, 1639–1643.
29 A. Dev, J. P. Richters, J. Sartor, H. Kalt, J. Gutowski and T. Voss, *Appl. Phys. Lett.*, 2011, **98**, 131111.
30 K. Vanheusden, C. H. Seager, W. L. Warren, D. R. Tallant and J. A. Voigt, *Appl. Phys. Lett.*, 1995, **68**, 403.
31 B. Alemán, Y. Ortega, J. Á. García, P. Fernández and J. Piqueras, *J. Appl. Phys.*, 2011, **110**, 014317.
32 B. K. Gupta, V. Rathee, T. N. Narayanan, P. Thanikaivelan, A. Saha, Govind, S. P. Singh, V. Shanker, A. A. Marti and P. M. Ajayan, *Small*, 2011, **7**, 1767–1773.
33 B. K. Gupta, P. Thanikaivelan, T. N. Narayanan, L. Song, W. Gao, T. Hayashi, A. L. M. Reddy, A. Saha, V. Shanker, M. Endo, A. A. Marti and P. M. Ajayan, *Nano Lett.*, 2011, **11**, 5227–5233.
34 S. K. Gupta, A. Joshi and M. Kaur, *J. Chem. Sci.*, 2010, **1**, 57–62.
35 V. D. Kapse, S. A. Ghosh, F. C. Raghuwanshi, S. D. Kapse and U. S. Khandekar, *Talanta*, 2009, **78**, 19–25.
36 B. Wang, L. F. Zhu, Y. H. Yang, N. S. Xu and G. W. Yang, *J. Phys. Chem. C*, 2008, **112**, 6643–6647.